Global and Planetary Change 174 (2019) 164–171

Contents lists available at ScienceDirect

Global and Planetary Change

journal homepage: www.elsevier.com/locate/gloplacha

Research Article

Spatially different responses of nitrogen processing to precipitation during glacial-interglacial cycles on the Chinese Loess Plateau

Zhiyang Li[a,e], Fajin Chen[b], Huili Liang[c], Guodong Jia[d,e,*]

[a] Guangdong AIB Polytechnic College, Guangzhou, China
[b] College of Ocean and Meteorology, Guangdong Ocean University, Zhanjiang, China
[c] Pearl River Fisheries Research Institute, Chinese Academy of Fishery Sciences, Guangzhou, China
[d] State Key Laboratory of Marine Geology, Tongji University, Shanghai, China
[e] Guangzhou Institute of Geochemistry, Chinese Academy of Sciences, Guangzhou, China

ARTICLE INFO

Keywords:
Organic nitrogen isotope
Precipitation
Loess-paleosol sequence
Chinese Loess plateau
Past climate change

ABSTRACT

Terrestrial nitrogen (N) cycling is closely associated with precipitation and crucial to ecosystem, which has been receiving great concerns at the backdrop of global climate change. In addition to modern investigations, paleo record of N cycling may provide valuable clues about how ecosystem N responds to climate change. Here we measured soil organic nitrogen (TON) and its isotope value ($\delta^{15}N_{org}$) in two loess-paleosol sequences (LPS), i.e. the Yuanbao (YB) and Luochuan (LC) sequences, on the Chinese Loess Plateau (CLP) accumulated during the glacial-interglacial cycles. Both sequences showed higher magnetic susceptibility in paleosol and lower in loess, but with overall higher values in the wetter site of LC, suggesting higher precipitation during warm periods for both sites, as well as higher precipitation at site LC than at site YB. TON increased with increase of paleo-precipitation in both sequences, but the fraction of microbial derived ON, estimated from $(C/N)_{org}$, increased faster than plant-derived ON at site YB but slower at site LC. $\delta^{15}N_{org}$ was used to estimate microbial mediated gaseous N loss, showing greater losses at higher paleo-precipitation at site YB and a reverse trend at site LC. Thereby, both $(C/N)_{org}$ and $\delta^{15}N_{org}$ suggest a quicker response of microbes than plants to precipitation at the drier site YB but conversely at the wetter site LC. Such a spatially different responses of nitrogen processing to precipitation would be a reference for projection of future terrestrial ecosystem response to climate change.

1. Introduction

Arid and semi-arid areas cover about 41% of Earth's land surface and are homes to > 38% of the total global population (Reynolds et al., 2007). The areas are also the hotspots for nitric oxides (NO_x) emissions (Homyak et al., 2016). The total area of dry lands is predicted to increase globally due to global warming and associated climate change (Dai, 2012; Trenberth et al., 2013). And more extreme climate will make arid and semi-arid ecosystems more drought (Trenberth et al., 2013). Changes in the magnitude of precipitation coupled with atmospheric nitrogen (N) deposition will exert profound impacts on cycling of terrestrial N, as well as carbon (C) (Gruber and Galloway, 2008; Harpole et al., 2007). It is a major challenge for ecologists to assess these impacts under future climate change and to develop effective adaptation strategies. Unraveling the association between paleo-precipitation pattern and N cycling during the past is helpful for understanding the impact of climate change in arid and semi-arid areas. Such a research could be fulfilled via retrieving associated records documented in the loess-paleosol sequence (LPS) on the Chinese Loess Plateau (CLP), which is accumulated during the glacial-interglacial climate cycles.

Natural abundance of N isotopes ($\delta^{15}N$) can provide insights into large-scale N dynamics in terrestrial ecosystems (Amundson et al., 2003; Chen et al., 2009; Houlton et al., 2006; Liu and Wang, 2008; Wang et al., 2014). In natural environments less influenced by human activities, N_2 fixation, as well as minor atmospheric N deposition, characterized by $\delta^{15}N$ of close to 0, are the main sources of N for terrestrial ecosystems (Houlton and Bai, 2009). During the terrestrial N cycling, ^{14}N is preferentially lost from an ecosystem via various pathways, such as volatilization, leaching, and N_2 emission during the course of denitrification, which may leave imprints on $\delta^{15}N$ retained in the ecosystem. The ecosystem $\delta^{15}N$ signal that integrates various N cycling processes in the past can be documented in soil organic matter (SOM), and thus revealed by measuring $\delta^{15}N$ of SOM ($\delta^{15}N_{org}$) in a

* Corresponding author at: State Key Laboratory of Marine Geology, Tongji University, Shanghai, China
E-mail address: jiagd@tongji.edu.cn (G. Jia).

https://doi.org/10.1016/j.gloplacha.2019.01.015
Received 24 August 2018; Received in revised form 24 January 2019; Accepted 28 January 2019
Available online 29 January 2019
0921-8181/ © 2019 Elsevier B.V. All rights reserved.

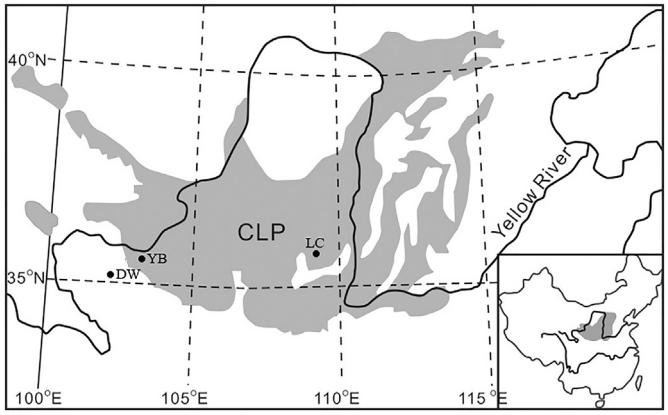

Fig. 1. Study area and sampling sites. The solid dots indicate the locations of sites Yuanbao (YB), and Luochuan (LC) in this study. Also shown is the site Duowa (DW) mentioned in this paper.

sediment sequence. In this study, we sampled two sections of LPS, covering a history up to 130 kyr, and measured $\delta^{15}N_{org}$ values in SOM. Our aim is to investigate the history of N cycling during the past climate change, which would be a valuable reference for understanding the current and future trend of N processes in arid and semi-arid areas.

2. Materials and methods

2.1. Sampling sites

Site Yuanbao (YB, 103°09′E, 35°38′N) is located on the western edge of the CLP with ca. 500 mm of mean annual precipitation (MAP), and site Luochan (LC, 109°25′E, 35°45′N) on the eastern CLP with ca. 620 mm of MAP (Fig. 1). Both sites are prevailed with a typical monsoon climate (Chen et al., 1997). Mean annual temperatures (MAT) at YB and LC sites are 7.0 °C and 9.2 °C, respectively, with winter temperature below freezing. Precipitation is concentrated from May to September, accounting for 80% of the MAP.

In this study, we investigated the upper 27 m of the YB sequence from the bottom of loess L1, accumulated during the last glacial time, to the paleosol S0, formed during the Holocene, with the top sample 0.5 m below the surface (Chen et al., 1997). The sequence was spliced by two exposed sections, CH02/02 and CH02/03, with 2–3 km apart (Jia et al., 2013). A total of 40 samples, 15 in the section CH02/02 and 25 in the section CH02/03 were collected. In the LC sequence, 38 samples were collected from the bottom of paleosol S1 formed during the last interglacial to the paleosol S0. In both sequences, there occurs a paleosol interlayer (L1SS1) in the middle part of the L1 section, hence separating L1 into an upper (L1LL1) and a lower (L1LL2) parts, respectively (Fig. 2).

2.2. Experiments

Each sample was oven dried at 50 °C, slightly grounded and one aliquot of ca. 8 g was analyzed using a Kappabridge MFK1-FA instrument for low- and high-field magnetic susceptibility (MS_L and MS_H, respectively). Percentage of frequency-dependent magnetic susceptibility (MS_F, %) was calculated according to following equation (Dearing et al., 1996):

$$MS_F = (MS_L - MS_H)/MS_L \times 100$$

Another aliquot of ca. 1.5 g was treated to concentrate total organic matter (TOM) according to Li and Jia (2011). Briefly, it was firstly treated with 1 M HCl to remove carbonate, then with 5 M HF/1 M HCl and 0.5 M HBO_3/0.5 M HCl to digest clay minerals. The final dark solid residue is mainly organic (Li and Jia, 2011). Dissolved organic material in the acid solutions was separately adsorbed onto a styrene divinyl benzene polymer (PPL) sorbent using solid phase extraction (0.5 g PPL cartridge, Varian) and was eluted with MeOH and acetone according to the procedure described by Dittmar et al. (2008). The combined elute was mixed with the acid-resistant solid residue to obtain TOM. After being thoroughly homogenized and freeze-dried, the TOM was weighed and measured for C and N content and $\delta^{15}N$ value using an elemental analysis-isotope ratio mass spectrometry (EA-IRMS) system (CEEA1112 C/N/S Analyzer interfaced with a DELTA-plus-XL mass spectrometer). A working standard material for $\delta^{15}N$ (urea with $\delta^{15}N$ + 0.4‰) was inserted between every 10 samples to monitor the working conditions of the analyzer. Reproducibility was ± 0.06% for total organic carbon (TOC), ± 0.02% for total organic nitrogen (TON), and ± 0.2‰ for $\delta^{15}N_{org}$ respectively. Blank analysis did not show detectable contamination during the whole experimental procedure. An aliquot of ca. 1.0 g in YB sequence was treated with 1 M HCl and dried to measure for total N content (TN, including total inorganic nitrogen (TIN) and TON). C/N ratio was calculated on mass basis.

3. Results

3.1. Age and magnetic susceptibility

The age of YB sequence was according to the OSL dating results (Lai and Wintle, 2006; Lai et al., 2007), and we applied the depth-age relationship (Jia et al., 2013; Lai et al., 2007) in this study. For the LC sequence, Porter and An (1995) has given a detailed age determination (Porter and An, 1995), which was applied here by MS correlation.

MS_L (10^{-8} m^3/kg) in the YB and LC sequence ranged from 27.93 to 146.97 (53.18 average) and from 52.09 to 254.13 (116.51 average), respectively, while MS_H (10^{-8} m^3/kg) ranged from 27.13 to 133.07 (50.17 average) and from 47.90 to 218.00 (102.26 average) (Fig. 2a), which are consistent with precious works (Jia et al., 2013; Porter and An, 1995). The MS_L and MS_H changed in parallel and showed lower values in loess and higher values in paleosol in the both sequences. MS_F in the YB sequence ranged from 0 to 10.43% (3.95% average), and that in the LC sequence from 8.04% to 14.22% (11.47% average) (Fig. 2b), also showing lower values in loess and higher values in paleosol in the both sequences. MS_L, MS_H and MS_F in the YB sequence were correspondingly lower than those in the LC sequence.

3.2. Variation of TOC, TON, TN, C/N ratio and $\delta^{15}N_{org}$ ratio

TOC content in the YB and LC sequences ranged from 0.31 mg/g to 8.47 mg/g and from 0.66 mg/g to 4.86 mg/g respectively (Fig. 2c). TON content ranged from 0.02 mg/g to 0.78 mg/g in the YB sequence and from 0.05 mg/g to 0.46 mg/g in the LC sequence (Fig. 2d). There were similar TOC and TON values between the two sequences. Both TOC and TON changed in parallel with MS and MS_F, showing lower values in L1 and higher values in S0 and S1. Even in the L1 deposit, they also showed slightly higher values in the L1SS1 paleosol. TOC and TON were prominently higher in S0 than in S1, due likely to less degradation in the younger S0. Organic C/N ratio ($(C/N)_{org}$) varied from 9.3 to 18.4 with an average of 13.1 in the YB sequence, and from 10.6 to 16. 8 with an average of 13.5 in the LC sequence (Fig. 2e). In the YB sequence, $(C/N)_{org}$ ratio was clearly lower in S0 than in L1, but this pattern did not occur in the LC sequence. TN content in the YB sequence ranged from 0.06 mg/g to 1.09 mg/g, while TIN accounted for 21.9%–85.5%, averaged on 56.1% (Fig. 3a). C_{org}/TN varied from 1.93 to 9.31 with an average of 5.55 in the YB sequence (Fig. 3b).

$\delta^{15}N_{org}$ value in YB and LC sequences ranged from 1.6‰ to 7.5‰ (4.2‰ average) and from 5.9‰ to 8.4‰ (7.1‰ average), respectively (Fig. 2f). In the YB sequence, $\delta^{15}N_{org}$ exhibited higher values in S0 than in L1, although several samples in L1SS1 also showed similarly higher values. In contrast, $\delta^{15}N_{org}$ exhibited slightly lower values in S0, L1SS1 and S1 than in L1LL1 and L1LL2 in the LC sequence.

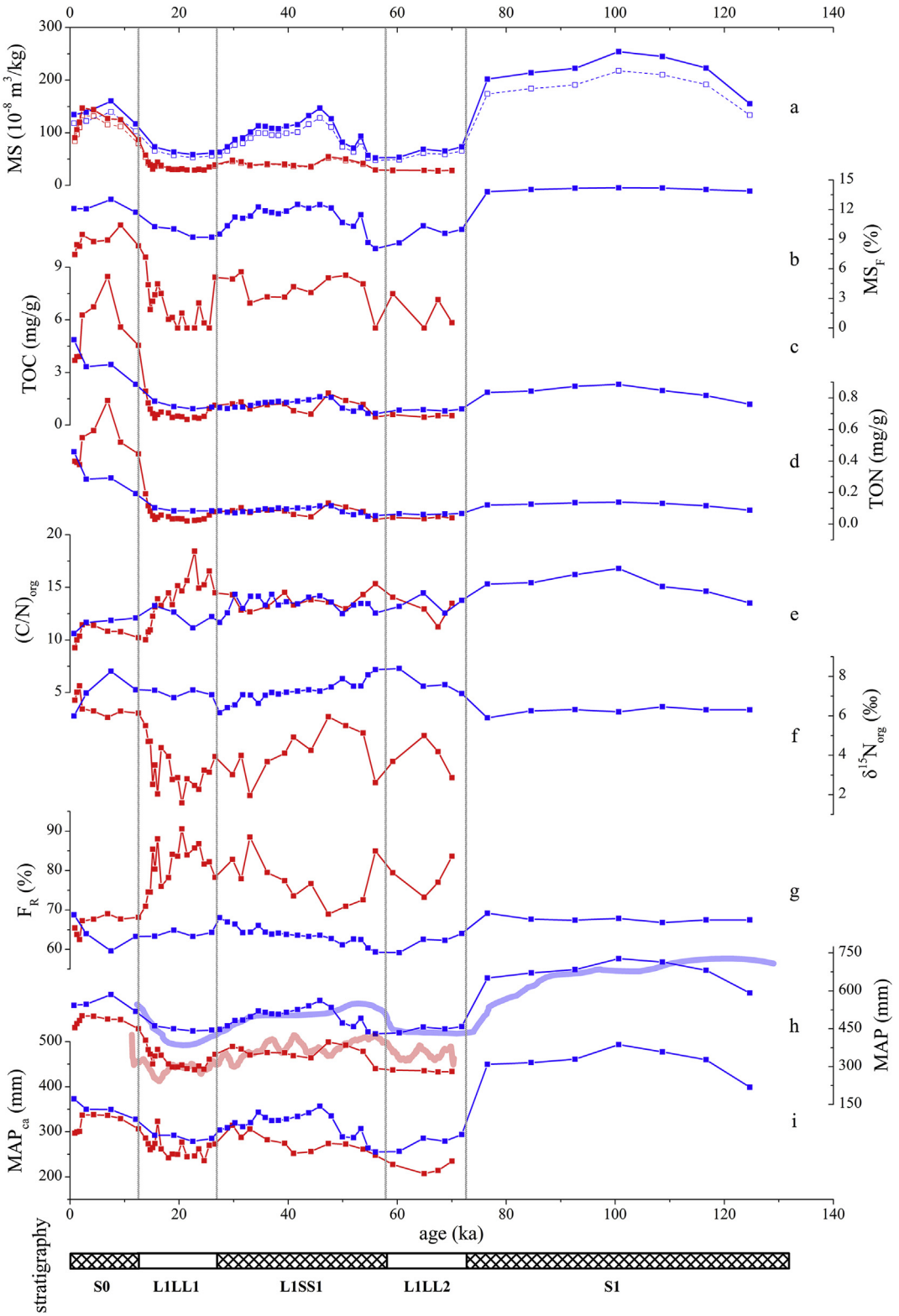

Fig. 2. Temporal variations of parameters in the two LPS. (a) MS_L (solid square) and MS_H (hollow square), (b) MS_F, (c) TOC, (d) TON, (e) $(C/N)_{org}$, (f) $\delta^{15}N_{org}$, (g) F_R, i.e., the fraction of N retained in the soil-plant system, (h) reconstructed MAPs. The light blue line stands for the paleo-precipitation which was reconstructed by Rb/Sr ratio (Chen et al., 2003; Li et al., 2007), and the light red line stands for the paleo-precipitation which was calculated by1.25 (summer precipitation occupied ca. 80% of the MAP) multiplied by the reconstructed summer paleo-precipitation by $\delta^{13}C$ (Rao et al., 2013), (i) MAP_{ca} (calculated by MAP multiplied by F_R). Red is for the YB sequence and blue for the LC sequence. (For interpretation of the references to colour in this figure legend, the reader is referred to the web version of this article.)

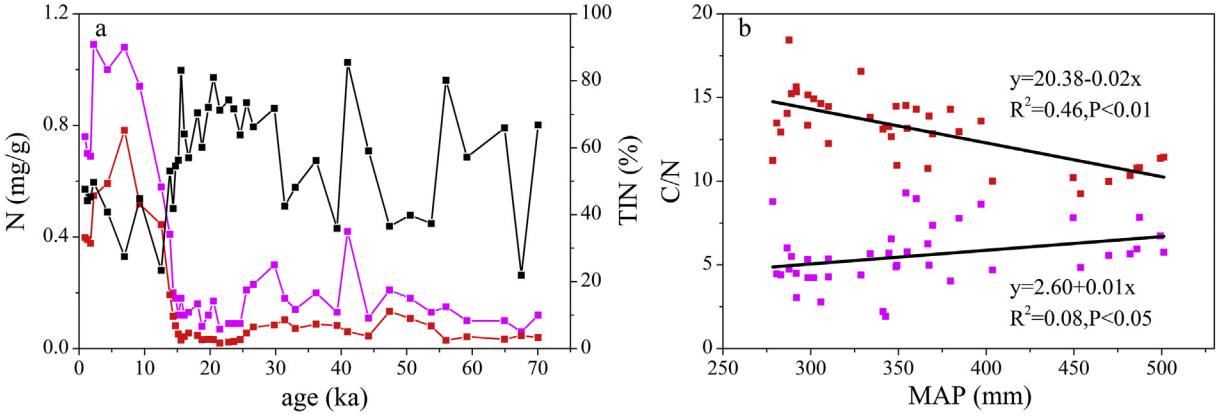

Fig. 3. (a) temporal variations of TN (pink), TON (red) and the contribution of TIN to TN (black) in the YB sequence; (b) $(C/N)_{org}$ (red) and C_{org}/TN (pink) against MAP in the YB sequence. (For interpretation of the references to colour in this figure legend, the reader is referred to the web version of this article.)

4. Discussion

4.1. Climate record

In East Asia, the glacial-interglacial climate cycles manifests themselves in the strength shift between East Asian winter monsoon (EAWM, stronger in the glacials) and summer monsoon (EASM, stronger in the interglacials) (e.g., Porter and An, 1995). The alternating occurrence of loess and paleosol in LPS on the CLP is the product of such climate cycles, with paleosol formed under stronger warm-humid EASM conditions and loess accumulated under stronger cold-dry EAWM conditions (Heller and Liu, 1986). The summer monsoon strength can be reflected by pedogenic process, which, among other factors, mainly controls the MS in the LPS (Zhou et al., 1990), and thus MS has been widely used as a proxy for EASM, and specifically for paleo-precipitation (Maher et al., 1994). Compared with MS, MS_F is mainly associated with soil iron oxides that is controlled by soil moisture budget, and is more reliable and sensitive to record the paleo-precipitation variations on different time-scales on the CLP (Heller and Liu, 1986; Liu et al., 1990; Liu et al., 1995; Liu et al., 2013; Maxbauer et al., 2016). Our results showed higher MS_F values in S0, L1SS1, S1 in both sequences (Fig. 2b), and thereby reflecting enhanced EASM during these periods, consistent with numerous previous results. Both MS and MS_F were clearly higher in the LC sequence than in the YB sequence, in agreement with presently higher MAT and MAP at site LC than at site YB and suggestive of a rough retention of such climatic offsets, albeit not constant, between localities during the glacial-interglacial cycles.

Precipitation is one of the most important monsoon climatic factors. Magnetic properties of the Chinese loess/paleosol sequences have been demonstrated to be controlled strongly by MAP (Liu et al., 2016). In order to quantitatively reconstruct paleo-precipation from the loess/paleosol sequences, many kinds of climofunctions have been established by linking precipitation to climatic proxies including stable oxygen isotope ($\delta^{18}O$) (Li et al., 2007), stable carbon isotope ($\delta^{13}C$) (Rao et al., 2013), and magnetic susceptibility (Han et al., 1996; Liu et al., 2016). Magnetic susceptibility-based methods are mostly applied, however, uncertainty might be large if they are not locally specific (Maher and Possolo, 2013). Accordingly, different susceptibility-based calibrations were used to reconstruct paleo-precipitation for the two sequences in this study. For the YB sequence, the climofunction of $MAP = 112 + 185 \times \log_{10}(MS_L - 20)$ ($R = 0.94$) established by Maher and Hu (2006) (Fig. 4a) was selected here because it was established for the Duowa sequence (Maher and Hu, 2006) close to the site YB (Fig. 1). For the LC sequence, a function of $MAP = 9.32 \times MS_{L\text{-}H} + 390.84$ has been approved applicable by Liu et al. (2016) (Fig. 4b), in which $MS_{L\text{-}H}$ is the difference between MS_L and MS_H (Liu et al., 2016). By inputting our MS data into the above two calibrations, respectively, MAPs were calculated, ranging from 430 mm to 727 mm (524 mm on average) in the LC sequence and from 278 mm to 501 mm (360 mm on average) in the YB sequence. Our results consist with the reconstructed results by stable carbon isotope ($\delta^{13}C$) and Rb/Sr ratio (Fig. 2h). Overall, MAPs of LC were higher than those of YB, consistent with present conditions. The paleo-precipitation data in the two sequences hereby constitute a precipitation series, which allowed us to examine soil N dynamics in response to a larger-range precipitation change, as will be done in the followings.

4.2. Contribution of higher plants vs. microbes to soil TOM

The TOC and TON records in both sequences changed in parallel with MS (Fig. 2c, d), consistent with numerous results reviewed by Zhao et al. (2009). But $(C/N)_{org}$ values here, mostly > 10, are clearly higher than previous results showing that C_{org}/TN ratio is usually < 10 (ranged from 2.40 to 11.85) (Zhang and Liu, 2008). This is because in previous studies N was total N, which included inorganic forms, mainly non-exchangeable ammonium fixed in the lattice of clay minerals. On the CLP, soil fixed ammonium has been found to account averagely for 29.7%–89.5% in total N (Dang et al., 2007). According to Rao et al. (2004), in the LC section, the content of fixed-ammonium N varied between 0.134 mg/g and 0.187 mg/g (Rao et al., 2004). In comparison, organic N in the LC section averaged 0.113 mg/g in this study. In the YB sequence, TIN accounted for 21.9%–85.5% (averaged on 56.1%), which led to smaller C_{org}/TN values (< 10) than $(C/N)_{org}$ values here. This difference further led to an opposite change trend against MAP of C_{org}/TN to that of $(C/N)_{org}$ (Fig. 3b). So, the substantial inorganic N trapped in clay minerals, which is not involved in soil nitrogen processes, may discount the application of bulk N to accurately reflect paleo N cycling in ecosystem. In our experiments, the interference of fixed N has been eliminated by removal of silicate. We believe organic N content and $\delta^{15}N_{org}$ here are more accurate to trace ecosystem N processes in the past.

$(C/N)_{org}$ ratio in soils could be influenced by sources of TOM and post depositional degradation of TOM. Soil TOM is sourced from two main groups of organisms: higher plants and microbes (Kogel-Knabner, 2002). Microbial biomass may be a significant source of TOM (> 50% of the extractable soil organic matter and > 80% of the soil nitrogen in some soils) and may initiate and enhance the formation of long-term stabilized TOM (Ludwig et al., 2015; Simpson et al., 2007). During glacial climate cycles, vegetation on the CLP is always dominated by herbs such as *Artemisia* and shrubs, and herbs decreased (i.e. shrubs increased) under colder and drier climate conditions (Jiang and Ding, 2005; Liu and Liu, 2017; Yang et al., 2015b). Three factors would affect the $(C/N)_{org}$ in sequences. The first factor may be the change in original C/N ratio of plants due to changes of nutrients and/or plant species

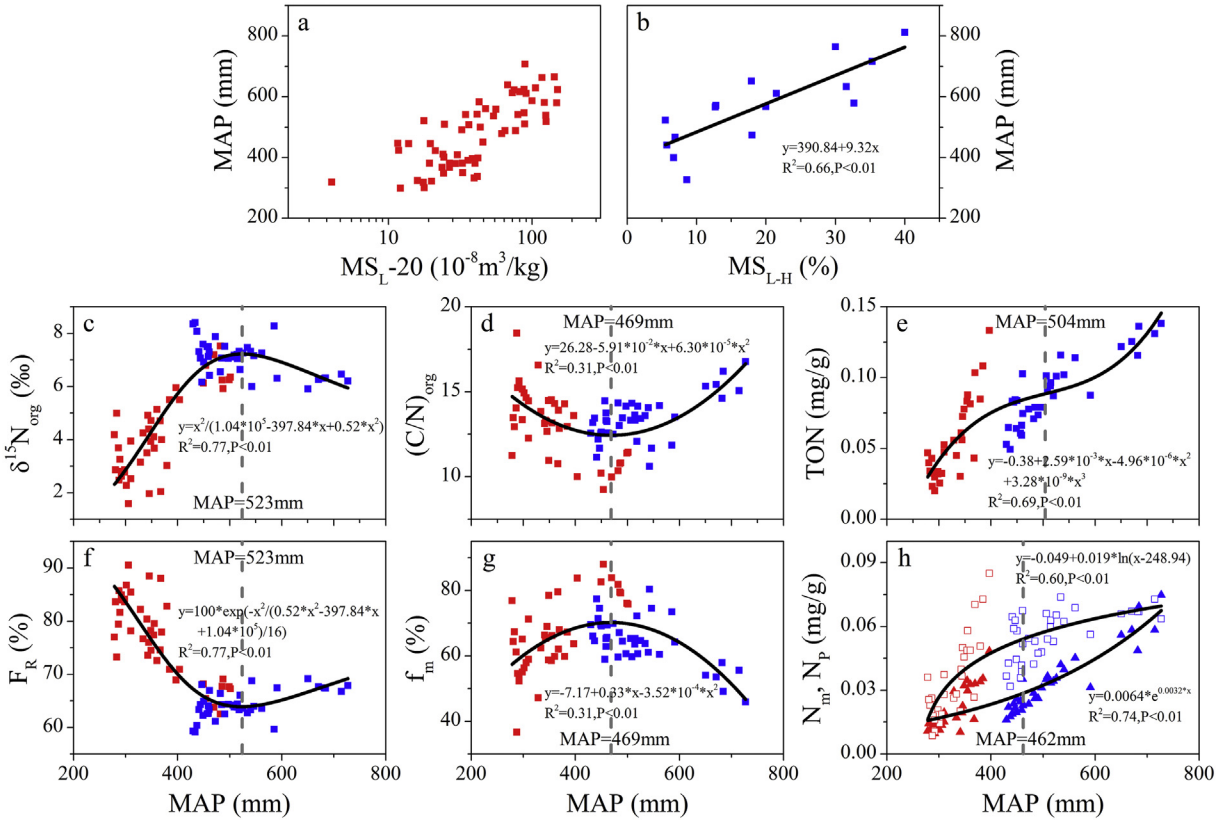

Fig. 4. Cross plots of (a) (MS_L − 20) modified by Maher and Hu (2006), (b) MS_{L-H} modified by Liu et al. (2016), (c) $\delta^{15}N_{org}$, (d) $(C/N)_{org}$, (e) TON, (f) F_R, (g) f_m, and (h) N_m (hollow square, calculated by TON * f_m), N_p (solid triangle, calculated by TON * (1 − f_m)) against MAP in the YB (red) and LC (blue) sequences. Samples showing prominently higher TON values due likely to less degradation in the younger soils were excluded in (e, h). (For interpretation of the references to colour in this figure legend, the reader is referred to the web version of this article.)

(mainly herbs and shrubs as described above) with climate change. However, modern vegetation investigations on the CLP show that leaf C/N ratio exhibits little difference between herbs (18.1 ± 6.0) and shrubs (19.7 ± 6.8) and no correlations with climatic conditions, including latitudes, MAT and MAP (Zheng and Shangguan, 2007). The relatively constant element ratio in plant litters, i.e., the organic matter input available for microbial decomposition and metabolism, suggests that soil microbes are also characterized by constant C/N ratio. So, the variation of $(C/N)_{org}$ ratio is also unlikely caused by changes in C/N ratio of microbes (or microbial residues). The change in C/N ratio of plant residues during degradation could be the second cause for variation of $(C/N)_{org}$ ratio down the soil profiles. The degree of degradation may be different between YB (dry and cold) and LC (wet and warm) and between during glacial periods (dry and cold) and during interglacial periods (wet and warm). Studies show that N content in the decomposing litter increases whereas C content decreases, leading to an exponential decrease to constant C/N ratios in stable plant residues after a long-time decomposition (Moore et al., 2006; Moore et al., 2010). And, the organic matter would be less degraded in dry-cold conditions than in wet-warm conditions, which should lead to higher $(C/N)_{org}$ values in the YB sequence than in the LC sequence, and higher values during the glacial periods than during the interglacial periods. However, our results were not exactly like that. Thereby, the change in C/N ratio of plant residues due to deferential degradation can be ruled out as a main cause for the $(C/N)_{org}$ down the two study sequences. Therefore, we believe the most likely cause is the third one, i.e., the change in the relative contribution of microbial and plant residues to soil TOM. By using the mean C/N values of microbial and plant residues as the end member values, the contribution of microbial residues to soil TOM (f_m) can be calculated according to the following equation:

$$R_{TOM} = R_m \cdot f_m + R_p \cdot (1 - f_m) \quad (1)$$

In the equation, R_{TOM} stands for the soil $(C/N)_{org}$ ratio, and R_m and R_p stand for C/N ratios of microbes and plant residues, respectively. Microbial C/N ratio is relatively constant at 7.1 ± 0.3 (Cleveland and Liptzin, 2007). But the ratio of plant residues, as well as its standard deviation, shows an exponential decrease from, for example, (64.7 ± 14.6) to (40.1 ± 10.1) and then to (30.2 ± 7.3) for the original litter C remaining of 100%–80%, 70%–50% and 40%–20%, respectively (Moore et al., 2006; Moore et al., 2010). According to the trend, at the 20% litter C remaining that approaches a relatively stable state, the C/N ratio of plant residue would be 25.0 (Moore et al., 2010) with a standar deviation of ± 5.5. Thereby, substituting R_m and R_p in Eq. (1) with 7.1 ± 0.3 and 25.0 ± 5.5, respectively, we obtained f_m values ranging from (36.7 ± 19.5)% to (88.0 ± 4.0)% with an average of (66.5 ± 10.4)% in the YB sequence and from (45.9 ± 16.6)% to (80.4 ± 6.2)% with an average of (64.5 ± 11.0)% in the LC sequence.

Overall the $(C/N)_{org}$ in the two sequences showed a quadratic polynomial relationship with MAP, showing a minimum value at a threshold of MAP = 469 mm (Fig. 4d). So the relative contribution of microbial residues to soil TOM showed an opposite trend with MAP (Fig. 4g), i.e., it increased with increasing MAP below the threshold (mostly in the YB sequence), and then decreased above the threshold (mostly in the LC sequence). Our results showed that both plant-derived ON (N_p) and microbial derived ON (N_m) increased with the increase of MAP in the two sequences. Here, the relationship between N_p and MAP can be described by an exponential function and that between N_m and MAP by a logarithmic function (Fig. 4h), which are consistent with modern investigations relating MAP with above-ground net primary productivity (Hu et al., 2007; Hu et al., 2010) and soil microbial

biomass (Li and Chen, 2004), respectively. As shown in Fig. 4h, however, the increasing rates of N_m and N_p showed opposite change trends, i.e. the increasing rate of N_m became lower and lower, while that of N_p became higher and higher, with the increase of MAP, and they were equal at MAP = 462 mm (Fig. 4h). Accordingly, we surmise that plant-microbe competition for inorganic N could be a mechanism for the different trends (Bontti et al., 2011; Dijkstra et al., 2012; Kaye and Hart, 1997). For the YB sequence (below the threshold), the climate was always drier than the LC sequence, soil microbes likely have been activated greater by precipitation than plants, leading to a positive correlation of microbial contribution with precipitation; whereas for the LC sequence (above the threshold), plants could have responded more rapidly than microbes, causing a depression of microbial activity and hence a negative trend of microbial contribution with the increase of precipitation (Bontti et al., 2011; Dijkstra et al., 2012; Kaye and Hart, 1997).

4.3. Mechanism of $\delta^{15}N_{org}$ variation

Plant (or microbes) N uptake does not express an appreciable isotope effect under natural N-limited soil conditions. This process causes a minimal isotopic difference between plant (or microbes) and its N source, and similarly does not significantly modify the isotopic ratio of the acquired N source (Hoch et al., 1994; Hogberg, 1997; Houlton et al., 2007). So the natural $\delta^{15}N$ of organic matter (microbial and plant residues) in loess-paleosol sequences can truly record the N processes in the past. Modern researches show that the natural $\delta^{15}N$ of soils and plants is correlated with environmental variables, most importantly climate (MAT and MAP), at both local and global scales (Amundson et al., 2003). However, the $\delta^{15}N$ values of modern plant roots and soil on the CLP show less significant relationships with MAT than with MAP, suggesting that MAP is the dominant factor for isotopic composition of plant-soil nitrogen (Liu and Wang, 2008). Here, our results showed a hump-shaped relationship between $\delta^{15}N_{org}$ and MAP with an inflection point at MAP = 523 mm, which is similar to the thresholds of precipitation for changes of $(C/N)_{org}$ and TON described above, albeit a little difference between them (Fig. 4c).

$\delta^{15}N$ of ecosystem may be determined by several factors: (i) atmospheric N input including N_2 fixation, (ii) leaching of N species, mainly nitrate, (iii) gaseous N loss to the atmosphere during the course of microbial N denitrification (Houlton et al., 2006), and (iiii) changes of vegetation species (Liu and Liu, 2017). Atmospheric N deposition and biological N_2 fixation are the external sources of N to the ecosystem, whose overall $\delta^{15}N$ is close to zero (Houlton and Bai, 2009). Nitrate leaching out of an ecosystem also exhibits only small isotope fractionation ($\varepsilon_L < -1‰$) (Houlton and Bai, 2009). However, the fact that $\delta^{15}N_{org}$ changed nonlinearly with precipitation in our results suggests that the two processes are not responsible for the variations of $\delta^{15}N_{org}$. Recently, Liu and Liu (2017) suggest the role of biological fixation on the variations of bulk $\delta^{15}N$ in a loess-paleosol sequence of Xifeng basing on the fact that the vegetation on the CLP is dominated by shrubs inclusive of leguminous plants during the glacials and by herbs that are all nonleguminous plants during the interglacials (Liu and Liu, 2017). This mechanism might be appropriate for the YB sequence because $\delta^{15}N$ variation record in the YB sequence is similar with the Xifeng sequence. However, it is not applicable to the LC sequence, in which $\delta^{15}N_{org}$ values were higher during the glacial time. Comparatively, gaseous N losses, an important N sink of ecosystem, may significantly influence soil $\delta^{15}N$ due to great isotope fractionations ($\varepsilon \approx -16‰$ to $-30‰$) (Robinson, 2001) with ^{14}N preferentially leaving the system. The clear positive $\delta^{15}N_{org}$ values of 1.6‰–8.4‰ in the study sequences indicate the overall predominance of gaseous N losses over atmospheric inputs and biological fixation in the past. Accordingly, gaseous losses could be a plausible candidate for the $\delta^{15}N_{org}$ variations observed here.

One pathway of gaseous N losses is ammonia volatilization, which may occur in alkaline soils on the CLP. However, we ruled out it as an important factor for $\delta^{15}N_{org}$ variations, because (1) in natural conditions, soil on CLP is nutrient deficient, implying rapid uptake by vegetation and microbes may overwhelm volatilization, and (2) ammonia volatilization may intensify, causing raise of $\delta^{15}N_{org}$ values, with elevated pH under conditions of decreased precipitation (Huang et al., 2008); however, $\delta^{15}N_{org}$ showed different trends with precipitation in the two sequences. Basing on above considerations, we finally prefer a gaseous N loss pathway via N_2 emission due to microbial denitrification as the cause of the observed $\delta^{15}N_{org}$ variations. As shown above, changes of the relative contribution of microbial derived ON exhibited different trends with the increase of precipitation (Fig. 4g), i.e., microbial contribution increased with elevated precipitation for the YB sequence, but decreased for the LC sequence. This occurrence implies that microbial mediated gaseous N losses may correspondingly increase, leading to elevated $\delta^{15}N_{org}$, with increase of precipitation at site YB, and conversely at site LC, which can reasonably interpret the different $\delta^{15}N_{org}$ variation patterns in our two study sites.

Here, the fraction of N retained in the ecosystem in the study sequences was calculated using an approximate form of the Rayleigh equation (Mariotti et al., 1981):

$$\delta^{15}N_R = \delta^{15}N_I + \varepsilon^* \ln F_R \quad (2)$$

$\delta^{15}N_R$ stands for the isotopes of residual N, equal to the measured value of $\delta^{15}N_{org}$; $\delta^{15}N_I$ stands for the input N isotope value, assumed to be 0‰; ε stands for the fractionation factor, assumed to be −16.0‰ in natural soils (Houlton and Bai, 2009); F_R stands for the fraction of N retained in the ecosystem. According Eq. (2), F_R value, showing an inverted hump-shaped relationship with MAP (Fig. 4f), ranged from 62.5% to 90.5% (77.1% on average) in the YB sequence and from 59.2% to 69.2% (64.3% on average) in the LC sequence (Fig. 2g). The averagely higher F_R values in the YB sequence, corresponding to the averagely lower $\delta^{15}N_{org}$ values, is attributable to weaker microbial N processing, under drier conditions than in the LC sequence. Higher F_R values mean less N loss from an ecosystem, which is favorable for primary production. N deposition responses linearly to precipitation (Li et al., 2015; Wang et al., 2014). The values of MAP * F_R are similar between the two sequences during L1 (Fig. 2i), which can explain the similar TOC and TON values during L1 (the higher values of TOC and TON and the difference between the two sequences during S0 may be due to the less degradation and different degradation rate), although it has been always drier at site YB than at site LC.

4.4. Implications for future N cycle of drylands

Global climate is undergoing a significant warming. Accompanying the global warming, there will be severe and widespread droughts over many land areas (Dai, 2012). Because most dryland soil is relatively infertile and the vegetation cover is sparse, dryland ecosystems are substantially more fragile (Reynolds et al., 2007). Knowledge of how climate change will affect the extent of drylands in the future is essential for the protection and for adaptation strategies.

Fundamentally, drought relates to the amount of water available in soils or hydrological systems (Trenberth et al., 2013). It is caused by either decreased precipitation and/or increased evaporation (Dai, 2012). Greatly amplifying evaporative demand due to temperature anomalies will increase the overall drought intensity, even though the annual precipitation is projected to increase across China (Chen and Sun, 2017), also in the northern China and on the dry CLP (Wu et al., 2015; Yang et al., 2015a). Based on the discussions above, precipitation is the dominant factor for N dynamics in the ecosystem on the CLP. For the twenty-first century, warming of 3.2–4.0 °C over drylands could occur when global warming reaches 2.0 °C (Huang et al., 2017). Assuming a ca. 10% increase in precipitation on the CLP under 3 °C warming target (Wu et al., 2015), the MAP at sites YB and LC will reach ca. 550 mm and ca. 682 mm, respectively. Based on our model (Fig. 4h), under these conditions N_m and N_p, respectively, will increase by 6.2%

and 17.4% at site YB, and by 4.6% and 21.9% at site LC.

5. Conclusions

Our results showed that C/N and $\delta^{15}N$ of soil TOM are useful indicators for reconstructing N cycling on the Chinese Loess Plateau. $(C/N)_{org}$ ratio is indicative of relative contributions of microbial derived N and plant-derived N to TOM, and $\delta^{15}N_{org}$ is suggestive of microbial mediated N loss from ecosystem. Both microbial and plant-derived N increased with the increase of MAP, but their increasing rates showed opposite change trends due to plant-microbe competition for inorganic N. This led to a hump-shaped relationship of microbial derived N with MAP, i.e., increasing at first in drier conditions and then decreasing in wetter conditions with a turning point at MAP = 469 mm. $\delta^{15}N_{org}$ of soil TOM also showed a similar hump-shaped relationship with MAP, which was associated with microbial mediated gaseous N losses. Gaseous N losses increase, leading to elevated $\delta^{15}N_{org}$, with the increase of precipitation bellow the precipitation threshold (in the YB sequence), and conversely above the threshold (in the LC sequence). Due to spatially different responses of nitrogen processing to precipitation on the Chinese Loess Plateau, microbial and plant derived N will increase differently at site YB and at site LC under global warming. These results will provide an important basis for predicting impacts of future climate change on the agroecological system.

Acknowledgements

This work was supported by the National Natural Science Foundation of China (Grant No. 41403003) and Project of Enhancing School with Innovation of Guangdong Ocean University (GDOU2013050201). Samples in the Yuanbao and Luochuan sequences were provided by Dr. Zhiguo Rao and Shiling Yang, respectively. Reviewers are thanked for their good comments.

References

Amundson, R., Austin, A.T., Schuur, E.A.G., Yoo, K., Matzek, V., Kendall, C., Ubersax, A., Brenner, D., Baisden, W.T., 2003. Global patterns of the isotopic composition of soil and plant nitrogen. Glob. Biogeochem. Cycles 17, 1031.

Bontti, E.E., Burke, I.C., Lauenroth, W.K., 2011. Nitrogen partitioning between microbes and plants in the shortgrass steppe. Plant Soil 342, 445–457.

Chen, H.P., Sun, J.Q., 2017. Anthropogenic warming has caused hot droughts more frequently in China. J. Hydrol. 544, 306–318.

Chen, F.H., Bloemendal, J., Wang, J.M., Li, J.J., Oldfield, F., 1997. High-resolution multi-proxy climate records from Chinese loess: evidence for rapid climatic changes over the last 75 kyr. Palaeogeogr. Palaeoclimatol. Palaeoecol. 130, 323–335.

Chen, Y., Chen, J., Liu, L.W., Ji, J.F., Zhang, J.X., 2003. Spatial and temporal changes of summer monsoon on the Loess Plateau of Central China during the last 130 ka inferred from Rb/Sr ratios. Science in China Series D 46, 1022–1030.

Chen, F.J., Jia, G.D., Chen, J.Y., 2009. Nitrate sources and watershed denitrification inferred from nitrate dual isotopes in the Beijiang River, South China. Biogeochemistry 94, 163–174.

Cleveland, C.C., Liptzin, D., 2007. C:N:P stoichiometry in soil: is there a “Redfield ratio” for the microbial biomass? Biogeochemistry 85, 235–252.

Dai, A.G., 2012. Increasing drought under global warming in observations and models. Nat. Clim. Chang. 3, 52–58.

Dang, Y.A., Li, S.Q., Wang, G.D., Shao, M.A., 2007. The different characteristics of soil fixed ammonium from south to north on the Loess Plateau. Plant Nutr. Fertil. Sci. 13, 831–837.

Dearing, J.A., Dann, R.J.L., Hay, K., Lees, J.A., Loveland, P.J., Maher, B.A., O'Grady, K., 1996. Frequency-dependent susceptibility measurements of environmental materials. Geophys. J. Int. 124, 228–240.

Dijkstra, F.A., Augustine, D.J., Brewer, P., Von Fischer, J.C., 2012. Nitrogen cycling and water pulses in semiarid grasslands: are microbial and plant processes temporally asynchronous? Oecologia 170, 799–808.

Dittmar, T., Koch, B., Hertkorn, N., Kattner, G., 2008. A simple and efficient method for the solid-phase extraction of dissolved organic matter (SPE-DOM) from seawater. Limnol. Oceanogr. Methods 6, 230–235.

Gruber, N., Galloway, J.N., 2008. An Earth-system perspective of the global nitrogen cycle. Nature 451, 293–296.

Han, J.M., Lü, H.Y., Wu, N.Q., Guo, Z.T., 1996. The magnetic susceptibility of modern soils in China and its use for paleoclimate reconstruction. Stud. Geophys. Geod. 40, 262–275.

Harpole, W.S., Potts, D.L., Suding, K.N., 2007. Ecosystem responses to water and nitrogen amendment in a California grassland. Glob. Chang. Biol. 13, 2341–2348.

Heller, F., Liu, T.S., 1986. Palaeoclimatic and sedimentary history from magnetic susceptibility of loess in China. Geophys. Res. Lett. 13, 1169–1172.

Hoch, M.P., Fogel, M.L., Kirchman, D.L., 1994. Isotope fractionation during ammonium uptake by marine microbial assemblages. Geomicrobiol J. 12, 113–127.

Hogberg, P., 1997. ^{15}N natural abundance in soil-plant systems. New Phytol. 137, 179–203.

Homyak, P.M., Blankinship, J.C., Marchus, K., Lucero, D.M., Sickman, J.O., Schimel, J.P., 2016. Aridity and plant uptake interact to make dryland soils hotspots for nitric oxide (NO) emissions. Proc. Natl. Acad. Sci. U. S. A. 113, 2608–2616.

Houlton, B.Z., Bai, E., 2009. Imprint of denitrifying bacteria on the global terrestrial biosphere. Proc. Natl. Acad. Sci. U. S. A. 106, 21713–21716.

Houlton, B.Z., Sigman, D.M., Hedin, L.O., 2006. Isotopic evidence for large gaseous nitrogen losses from tropical rainforests. Proc. Natl. Acad. Sci. U. S. A. 103, 8745–8750.

Houlton, B.Z., Sigman, D.M., Schuur, E.A.G., Hedin, L.O., 2007. A climate-driven switch in plant nitrogen acquisition within tropical forest communities. Proc. Natl. Acad. Sci. U. S. A. 104, 8902–8906.

Hu, Z.M., Fan, J.W., Zhong, H.P., Yu, G.R., 2007. Spatiotemporal dynamics of aboveground primary productivity along a precipitation gradient in Chinese temperate grassland. Sci. China Ser. D Earth Sci. 50, 754–764.

Hu, Z.M., Yu, G.R., Fan, J.W., Zhong, H.P., Wang, S.Q., Li, S.G., 2010. Precipitation-use efficiency along a 4500-km grassland transect. Glob. Ecol. Biogeogr. 19, 842–851.

Huang, D.K., Lee, X.Q., Jiang, W., Zhao, Y.L., Ding, W.C., 2008. Geographic variation of carbonate content and pH in surface soil in East Central Asia: significance as climate proxies. Geochimica 37, 129–138.

Huang, J.P., Yu, H.P., Dai, A.G., Wei, Y., Kang, L.T., 2017. Drylands face potential threat under 2°C global warming target. Nat. Clim. Chang. 7, 417–422.

Jia, G.D., Rao, Z.G., Zhang, J., Li, Z.Y., Chen, F.J., 2013. Tetraether biomarker records from a loess-paleosol sequence in the western Chinese Loess Plateau. Front. Microbiol. 4, 199.

Jiang, H.C., Ding, Z.L., 2005. Temporal and spatial changes of vegetation cover on the Chinese Loess Plateau through the last glacial cycle: evidence from spore-pollen records. Rev. Palaeobot. Palynol. 133, 23–37.

Kaye, J.P., Hart, S.C., 1997. Competition for nitrogen between plants and soil microorganisms. Trends Ecol. Evol. 12, 139–143.

Kogel-Knabner, I., 2002. The macromolecular organic composition of plant and microbial residues as inputs to soil organic matter. Soil Biol. Biochem. 34, 139–162.

Lai, Z.P., Wintle, A.G., 2006. Locating the boundary between the Pleistocene and the Holocene in Chinese loess using luminescence. The Holocene 16, 893–899.

Lai, Z.P., Wintle, A.G., Thomas, D.S.G., 2007. Rates of dust deposition between 50 ka and 20 ka revealed by OSL dating at Yuanbao on the Chinese Loess Plateau. Palaeogeogr. Palaeoclimatol. Palaeoecol. 248, 431–439.

Li, X.Z., Chen, Z.Z., 2004. Soil microbial biomass C and N along a climatic transect in the Mongolian steppe. Biol. Fertil. Soils 39, 344–351.

Li, Z.Y., Jia, G.D., 2011. Separation of total nitrogen from sediments into organic and inorganic forms for isotopic analysis. Org. Geochem. 42, 296–299.

Li, G.G., Sheng, X.F., Chen, J., Yang, J.D., Chen, Y., 2007. Oxygen-isotope record of paleorainwater in authigenic carbonates of Chinese loess-paleosol sequences and its paleoclimatic significance. Palaeogeogr. Palaeoclimatol. Palaeoecol. 245, 551–559.

Li, X.L., Shi, H.Q., Xu, W.F., Liu, W., Wang, X.J., Hou, L.Y., Feng, F., Yuan, W.P., Li, L.H., Xu, H., 2015. Seasonal and spatial variations of bulk nitrogen deposition and the impacts on the carbon cycle in the arid/semiarid grassland of inner Mongolia, China. PLoS One 10 e0144689.

Liu, J.C., Liu, W.G., 2017. Soil nitrogen isotopic composition of the Xifeng loess-paleosol sequence and its potential for use as a paleoenvironmental proxy. Quat. Int. 440, 35–41.

Liu, W.G., Wang, Z., 2008. Nitrogen isotopic composition of plant-soil in the Loess Plateau and its responding to environmental change. Science Bulletin 54, 272–279.

Liu, X.M., Liu, T.S., Heller, F., Xu, T.C., 1990. Frequency-dependent susceptibility of loess and quaternary paleoclimate. Quat. Sci. 10, 42–50.

Liu, X.M., Rolph, T., Bloemendal, J., Shaw, J., Liu, T.S., 1995. Quantitative estimates of palaeoprecipitation at Xifeng, in the Loess Plateau of China. Palaeogeogr. Palaeoclimatol. Palaeoecol. 113, 243–248.

Liu, Z.F., Liu, Q.S., Torrent, J., Barrón, V., Hu, P.X., 2013. Testing the magnetic proxy χFD/HIRM for quantifying paleoprecipitation in modern soil profiles from Shaanxi Province, China. Glob. Planet. Chang. 110, 368–378.

Liu, Z.F., Wei, G.J., Wang, X.S., Jin, C.S., Liu, Q.S., 2016. Quantifying paleoprecipitation of the Luochuan and Sanmenxia Loess on the Chinese Loess Plateau. Palaeogeogr. Palaeoclimatol. Palaeoecol. 459, 121–130.

Ludwig, M., Achtenhagen, J., Miltner, A., Eckhardt, K.-U., Leinweber, P., Emmerling, C., Thiele-Bruhn, S., 2015. Microbial contribution to SOM quantity and quality in density fractions of temperate arable soils. Soil Biol. Biochem. 81, 311–322.

Maher, B.A., Hu, M.Y., 2006. A high-resolution record of Holocene rainfall variations from the western Chinese Loess Plateau: antiphase behaviour of the African/Indian and East Asian summer monsoons. The Holocene 16, 309–319.

Maher, B.A., Possolo, A., 2013. Statistical models for use of palaeosol magnetic properties as proxies of palaeorainfall. Glob. Planet. Chang. 111, 280–287.

Maher, B.A., Thompson, R., Zhou, L.P., 1994. Spatial and temporal reconstructions of changes in the Asian palaeomonsoon: a new mineral magnetic approach. Earth Planet. Sci. Lett. 125, 461–471.

Mariotti, A., Germon, J.C., Hubert, P., Kaiser, P., Letolle, R., Tardieux, A., Tardieux, P., 1981. Experimental determination of nitrogen kinetic isotope fractionation: some principles; illustration for the denitrification and nitrification processes. Plant Soil 62, 413–430.

Maxbauer, D.P., Feinberg, J.M., Fox, D.L., 2016. Magnetic mineral assemblages in soils and paleosols as the basis for paleoprecipitation proxies: a review of magnetic methods and challenges. Earth Sci. Rev. 155, 28–48.

Moore, T.R., Trofymow, J.A., Prescott, C.E., Fyles, J., Titus, B.D., 2006. Patterns of carbon, nitrogen and phosphorus dynamics in decomposing foliar litter in Canadian forests. Ecosystems 9, 46–62.
Moore, T.R., Trofymow, J.A., Prescott, C.E., Titus, B.D., 2010. Nature and nurture in the dynamics of C, N and P during litter decomposition in Canadian forests. Plant Soil 339, 163–175.
Porter, S.C., An, Z.S., 1995. Correlation between climate events in the North Atlantic and China during the last glaciation. Nature 375, 305–308.
Rao, W.B., Luo, T.Y., Gao, Z.M., Li, X.B., 2004. Paleoclimatic significance of fixed-NH_4^+-N in the Luochuan loess section during the last 130ka. Geochimica 33, 185–190.
Rao, Z.G., Chen, F.H., Cheng, H., Liu, W.G., Wang, G.A., Lai, Z.P., Bloemendal, J., 2013. High-resolution summer precipitation variations in the western Chinese Loess Plateau during the last glacial. Sci. Rep. 3, 2785.
Reynolds, J.F., Smith, D.M., Lambin, E.F., Turner II, B.L., Mortimore, M., Batterbury, S.P.J., Downing, T.E., Dowlatabadi, H., Fernández, R.J., Herrick, J.E., Huber-Sannwald, E., Jiang, H., Leemans, R., Lynam, T., Maestre, F.T., Ayarza, M., Walker, B., 2007. Global desertification: building a science for dryland development. Science 316, 847–851.
Robinson, D., 2001. $\delta^{15}N$ as an integrator of the nitrogen cycle. Trends Ecol. Evol. 16, 153–162.
Simpson, A.J., Simpson, M.J., Smith, E., Kelleher, B.P., 2007. Microbially derived inputs to soil organic matter: are current estimates too low? Environ. Sci. Technol. 41, 8070–8076.
Trenberth, K.E., Dai, A.G., Schrier, G., Jones, P.D., Barichivich, J., Briffa, K.R., Sheffield, J., 2013. Global warming and changes in drought. Nat. Clim. Chang. 4, 17–22.
Wang, C., Wang, X.B., Liu, D.W., Wu, H.H., Lü, X.T., Fang, Y.T., Cheng, W.X., Luo, W.T., Jiang, P., Shi, J., Yin, H.Q., Zhou, J.Z., Han, X.G., Bai, E., 2014. Aridity threshold in controlling ecosystem nitrogen cycling in arid and semi-arid grasslands. Nat. Commun. 5, 4799.
Wu, J., Zhou, B.T., Xu, Y., 2015. Response of precipitation and its extremes over China to warming: CMIP5 simulation and projection. Chin. J. Geophys. 58, 461–473.
Yang, S.L., Ding, Z.L., Li, Y.Y., Wang, X., Jiang, W.Y., Huang, X.F., 2015a. Warming-induced northwestward migration of the East Asian monsoon rain belt from the Last Glacial Maximum to the mid-Holocene. Proc. Natl. Acad. Sci. U. S. A. 112, 13178–13183.
Yang, X.X., Jiang, W.Y., Yang, S.L., Kong, Z.C., Luo, Y.L., 2015b. Vegetation and climate changes in the western Chinese Loess Plateau since the Last Glacial Maximum. Quat. Int. 372, 58–65.
Zhang, P., Liu, W.G., 2008. Loess sedimentary organic matter records from the central Chinese Loess Plateau and the implication of C/N. Mar. Geol. Quat. Geol. 28, 119–124.
Zhao, Y., Yu, Z.C., Chen, F.H., Zhang, J.W., Yang, B., 2009. Vegetation response to Holocene climate change in monsoon-influenced region of China. Earth Sci. Rev. 97, 242–256.
Zheng, S.X., Shangguan, Z.P., 2007. Spatial patterns of leaf nutrient traits of the plants in the Loess Plateau of China. Trees 21, 357–370.
Zhou, L.P., Oldfield, F., Wintle, A.G., Robinson, S.G., Wang, J.T., 1990. Partly pedogenic origin of magnetic variations in Chinese loess. Nature 346, 737–739.